Multiscale EMC Modeling, Simulation, and Validation of a Synchronous Step-Down DC-DC Converter

Rajen Murugan, *Senior Member, IEEE*, Jie Chen, *Member, IEEE*, Ambreesh Tripathi, Bibhu Prasad Nayak, *Member, IEEE*, Harikiran Muniganti, and Dipanjan Gope, *Senior Member, IEEE*

***Abstract*—The proliferation of power electronics in automotive and industrial applications raises compliance challenges in meeting electromagnetic compatibility (EMC) regulatory standards. In this work, we develop a robust multiscale system-level modeling and simulation methodology for predicting CISPR 25 conducted emission (CE) and radiated emission (RE). The method is based on a novel two-stage process. In the first stage, the IC model is generated either by non-linear time-domain simulation using a device-level physics model or oscilloscope measurements if a prototype is available. In the second stage, the IC model waveforms are used in a simulation environment comprising 3D full-wave frequency domain analysis and specially prepared macro-models for the laboratory equipment. Silicon validation of CISPR 25 EMC measurements on a "low-EMI," high-performance DCDC automotive/industrial synchronous step-down converter is presented to validate the integrity of the predictive modeling methodology. Good correlations between modeling and EMC-certified testing laboratory emission measurements are achieved (i.e., within +/- 3 dBuV for CE and +/- 6 dBuV for RE). As a result, the predictive EMC modeling methodology can be implemented, early in the design cycle, to ensure first-pass EMC-compliant design.**

***Index Terms*—Automotive, CISPR25, DCDC, EMC, method of moments, multiscale, system-level.**

I. Introduction

BY VIRTUE of their inherent design, switch-mode power converters generate electromagnetic interference and are also susceptible to emissions. These converters must comply with their electromagnetic environment, which must adhere to emission limits imposed by the regulatory standards (e.g., CISPR, ISO, and SAE). The ability to achieve electromagnetic compliance (EMC) is worsening as low emissions and high immunity to interference have emerged as key differentiators in the performance selection of power converters. In addition, the EMC challenges have been exacerbated by the industry's drive for higher efficiency and low-cost solutions through the adoption of advanced semiconductor process integration [1], higher switching speed converters [2], [3], and higher-level of components integration and form-factor reduction [4], [5].

CISPR 25 is a system-level specification that sets limits for conducted (150 kHz–108 MHz) and radiated emissions (150 kHz–2.5 GHz) of automotive components and modules [6]. From an automotive electronic product designer's perspective, meeting regulatory compliance to CISPR 25 EMC standard is critical as the efforts required can potentially impact product development costs and time to market. As such, the ability to predict emissions through modeling and simulation early in the product design phase is of utmost importance. However, despite the availability of current state-of-art mature three-dimensional (3D) full-wave electromagnetic solutions, the ability to perform multiscale system-level EMC predictive modeling and analysis has been mostly elusive. The limitations are typically associated with the complexity of fully modeling the whole system (i.e., silicon + package + PCB systems) [7], the excessively lengthy computing time [8], and the ever-shortening design cycle time [9]. Therefore, a multiscale modeling methodology is needed to provide solver technologies for dimensions ranging from nanometer scale for the power transistors to micrometer for the die size, millimeters for the package, and centimeters for the PCB system, and meters for the anechoic EMC test chamber is critical. In addition, the lack of standardized models that capture the realistic interactions of the non-linear time-variant power switcher effect and its electromagnetic interactions with the system pose severe challenges to the modeling and predicting device EMC performance.

Several methods have been attempted despite these challenges, as evident in the literature. Current techniques either focus solely on conducted emission predictive methods [10], [11], limited applicability of behavior-based models [12], [13], time-excessive transfer function-based approaches [14], [15], [16] or radiated emission only [17], [18], and [19]. Additionally, existing system-level/virtual lab modeling approaches that coupled circuit-to-electromagnetic methods tend to adopt measurement-based behavioral modeling to model the switcher with limited applicability [14], [20], [21], [22], [23] and [24].

Manuscript received 22 August 2022; revised 30 November 2022; accepted 31 March 2023. Date of publication 5 June 2023; date of current version 11 August 2023. *(Corresponding author: Dipanjan Gope.)*

Rajen Murugan and Jie Chen are with Texas Instruments, Inc., Dallas, TX 75243 USA (e-mail: rajenm@ieee.org; jchen_j@ti.com).

Ambreesh Tripathi is with Texas Instruments, Inc., Santa Clara, CA 95051 USA (e-mail: ambreesh@ti.com).

Bibhu Prasad Nayak and Harikiran Muniganti are with Simyog Technology Private Limited, Bengaluru 560034, India (e-mail: bibhu@simyog.com; harikiran@simyog.com).

Dipanjan Gope is with the Electrical Communication Engineering Department, Indian Institute of Science, Bangalore 560012, India (e-mail: dipanjan@iisc.ac.in).

Digital Object Identifier 10.1109/JMMCT.2023.3276358

In [25], a PCB-only approach toward magnetic near-field calculations is adopted. This does not capture cable, LISN, antenna, and other laboratory effects of CISPR25.

This work develops a multiscale system-level EMC predictive modeling methodology that is comprised of two stages. In the first stage, the noise waveform characteristic of the IC, also called the IC-model, is obtained. This can be done using an oscilloscope measurement if a PCB prototype is available. Otherwise, a non-linear time-domain simulation, including the PCB, package, components, and the IC's device-level physics model may be used. It is also demonstrated that adding cable, LISN, and any other laboratory equipment does not change the obtained waveform. In the second stage, the IC-model is used in a 3D full-wave solver environment where pre-characterized LISN, antenna, and EMI-receiver models are used. The methodology encompasses varying scales, e.g., IC, package, PCB system, EMC antenna, table, and chamber. Further, it covers different physical treatments, including non-linear circuit simulation for the IC and linear electromagnetic simulation for the rest of the system. Finally, the robustness and accuracy of the modeling methodology are demonstrated on an automotive synchronous step-down converter and validated with measured data for CISPR 25 EMC compliance.

The article is organized as follows. Section II summarizes the device-under-test (DUT) key features (i.e., the automotive synchronous step-down DC-DC converter) and discusses the sources and mechanisms of emission inherent to the DUT. The complete multiscale modeling and simulation methodology is presented in Section III. In Section IV, the CISPR 25 EMC laboratory test environment is detailed. Finally, the comparative simulation to measurements correlation data is presented, and findings are discussed in Section V.

II. Automotive Synchronous Step-Down Converter

The device-under-test (DUT) selected for this work is an automotive-focused, DC-DC synchronous step-down converter (Fig. 1). With integrated high-side and low-side MOSFETs, up to 4A output current is delivered over a wide input range of 3.0V to 36V. The design is customized for minimal EMI. It incorporates a pseudo-random spread spectrum, adjustable SW node rise time, a low-EMI VQFN-HR package [26] featuring low switch-node (SW) ringing, and optimized pinout for ease of use. The frequency the device can switch has been synchronized between 200 kHz and 2.2 MHz to avoid noise-sensitive frequency bands. Additionally, it is AEC-Q100-qualified and can operate up to a maximum junction temperature of 150 °C.

In a typical automotive end equipment (EE), a wide input front-end synchronous step-down converter, e.g., the DUT, converts the unregulated battery voltage to a regulated step-down voltage. The power requirement of such converters can range from sub-1W to a few kW, depending on the application's need. These converters face many unique challenges related to automotive applications. These include large voltage transients due to load dump; large voltage undershoots during cold and warm crank; low quiescent current; high ambient junction temperature (up to 150 °C); and the need to comply with growing stringent CISPR 25 Class 5 EMI compliance requirements.

Today's automotive systems with extended wire harness and miniaturized sizes support higher computational power. These emerging challenges mean that the front-end synchronous buck converters must handle higher processing power and switch at higher frequencies, creating high dv/dt and di/dt transients that impacting system EMC performance. As such, a clear understanding of the sources of the EMI noise is critical for optimal EMC design.

EMI is one of the most undesired effects of any synchronous step-down converter. The primary noise sources in such a converter involve discontinuous input currents due to the switching of power field-effect transistors (FETs), the fast-rising and falling rate of the switch/phase node, and additional ringing along the switching edges due to parasitic inductance and capacitances in the gate and power loops (Fig. 2) [27]. Typically, the noise sources can be classified into the following four categories:

1) *Conducted path through the DC input side* – seen as glitches/ringing on supply rails require filtering – e.g., decoupling, common-mode choke, ferrite bead. High-frequency noise current from LC resonance of switching loop [28], [29] coupled to the DC input side and is synchronous to the switch SW/phase voltage waveform.
2) *Conducted path through the DC output side* – due to the impedance of the main inductor and heavy capacitive loading on the output side, likely no significant noise is observed on the output rails.
3) *Electric coupling from the SW/phase node voltage* – due to capacitive coupling from the SW node to the PCB routing. The SW pin of the buck converter has high dv/dt and high harmonics at high frequencies. This causes high-frequency noise to couple to PCB and creates high dv/dt loops [30], [31].
4) *Magnetic coupling from the switching loop* – due to the high di/dt magnetic coupling from the switching loop. Magnetic field coupling is modeled as mutual inductance. The high-frequency harmonics in the input current generate a magnetic field, which jumps over the input EMI filters and couples to the LISN. Another magnetic noise source is the power inductor [32].

III. Multiscale Modeling Methodology

Predicting the EMC performance of the Design-Under-Test (DUT) through modeling and simulation involves specific challenges, especially concerning the multiscale and multi-physics aspects of different components affecting the accuracy of the simulation. The integrated circuits on the DUT must be characterized accurately to quantify the non-linear switching behavior as they are the primary source of electromagnetic noise. The package, printed circuit board (PCB), harness, LISN, and table form the pathway for current flow. For radiated emissions, the antenna may sometimes be coupled to the DUT and harness at lower frequencies and, therefore must be modeled accurately for precise results. In addition, measurement-to-simulation correlation is more complicated for radiated emission with chamber-to-chamber variations. This section describes the modeling methodology for a multiscale modeling approach to capture the EMI noise sources.

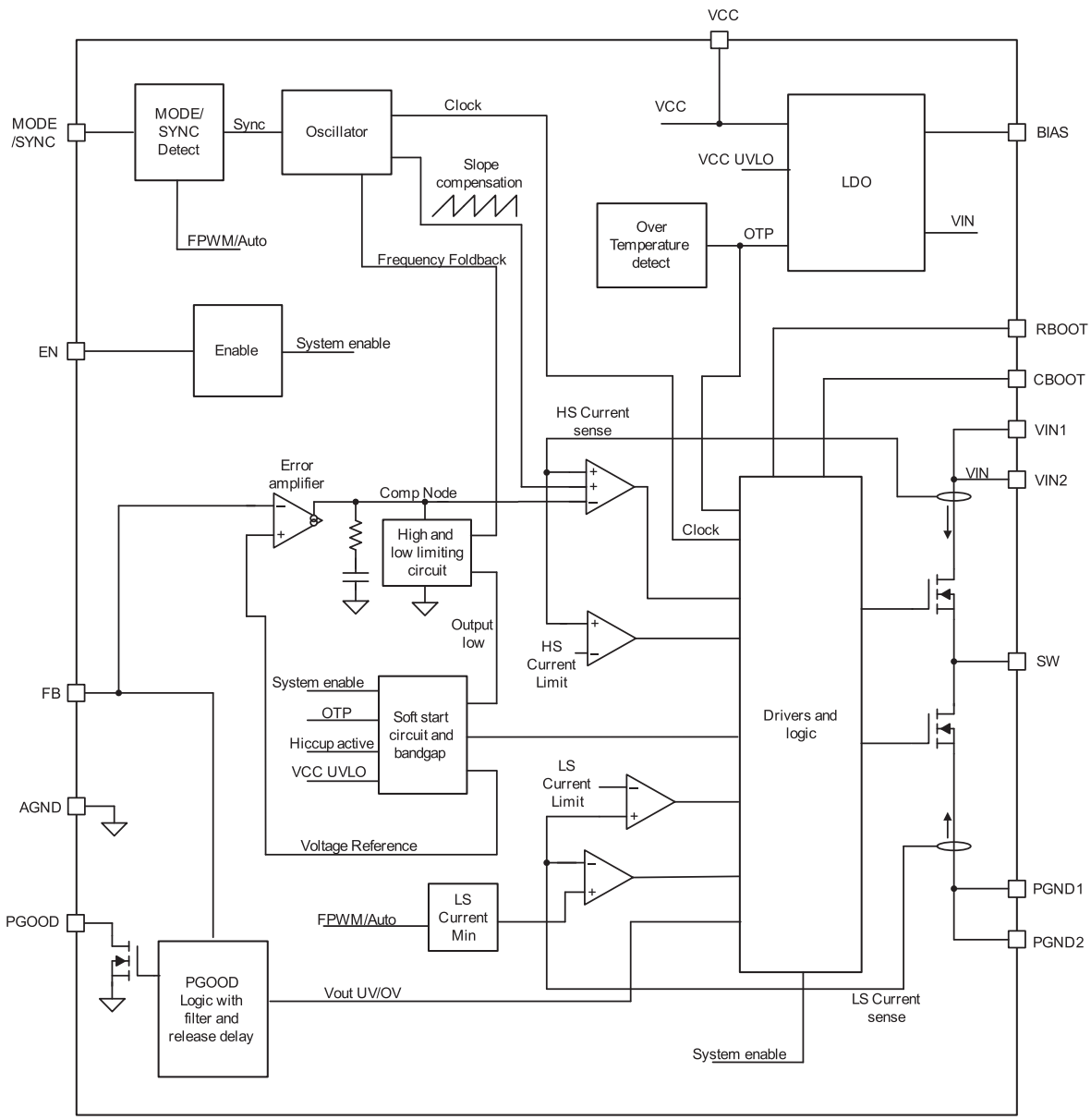

Fig. 1. Functional block diagram of the automotive synchronous step-down converter.

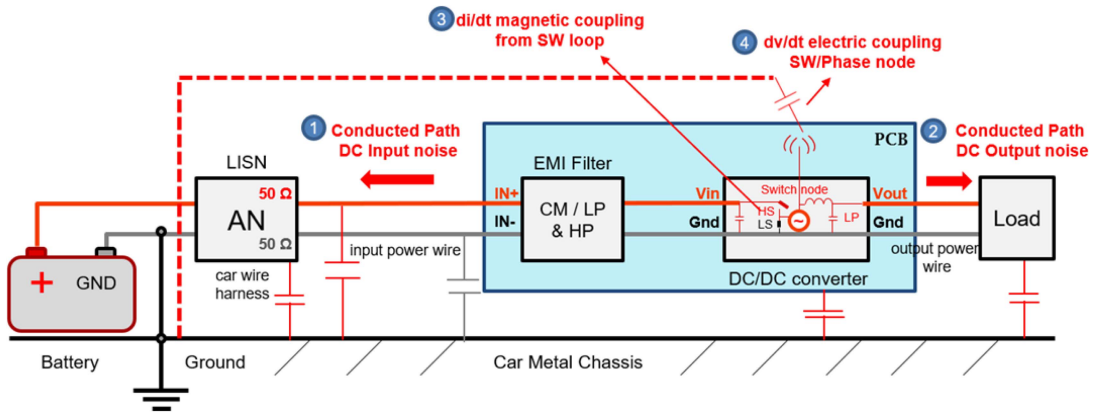

Fig. 2. Typical sources of noise in a synchronous step-down DC-DC converter.

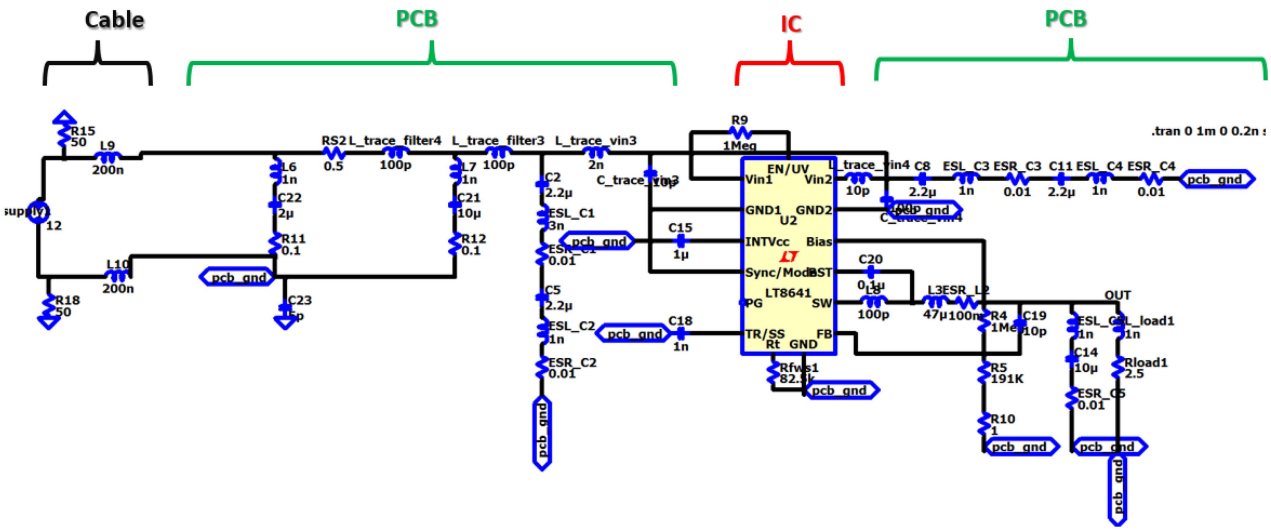

(a)

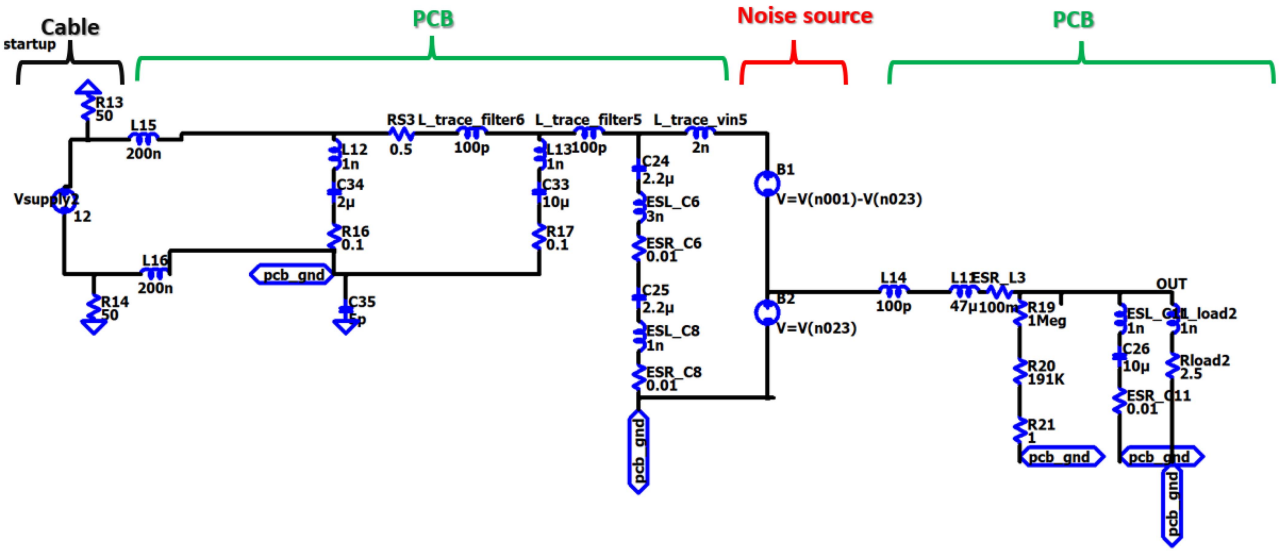

(b)

Fig. 3. The non-linear blocks of the PCB are characterized using equivalent sources: (a) Schematic diagram of the PCB with the actual IC (b) schematic diagram of PCB with equivalent sources.

A. *Stage-1: IC-Model Generation*

The objective in this stage is to capture the noise waveforms resulting from the switching of the MOSFETs inside the IC. As shown in Fig. 3, the non-linear IC-block can be replaced by equivalent sources to be used in Stage-2.

1) Measurement-Based Approach: The IC-model waveforms may be obtained using oscilloscope measurements if a prototype of the PCB is available. Further, the measurements need not be performed in the laboratory setting, and a stand-alone PCB measurement is adequate. This is also demonstrated in the following sub-section. Fig. 4 shows such a measurement setup.

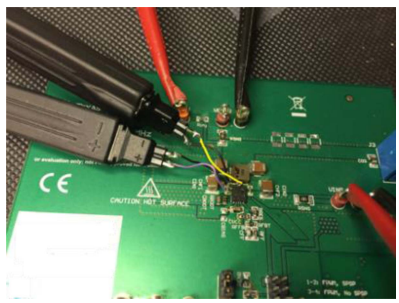

Fig. 4. PCB-level measurements with an oscilloscope and active probe.

2) Simulation-Based Approach: A more useful pre-prototype methodology for obtaining the IC model is performing a non-linear complete transient analysis. Fig. 5 shows the multiscale system-level connectivity of the transient analysis. The high-side and low-side MOSFET switches of the source-synchronous device are modeled accurately to capture their impact on both conducted and radiated EMI. The intrinsic non-linearity of the MOS gate capacitances dependence on Vgs (gate-to-source voltage) and Vds (drain-to-source voltage)

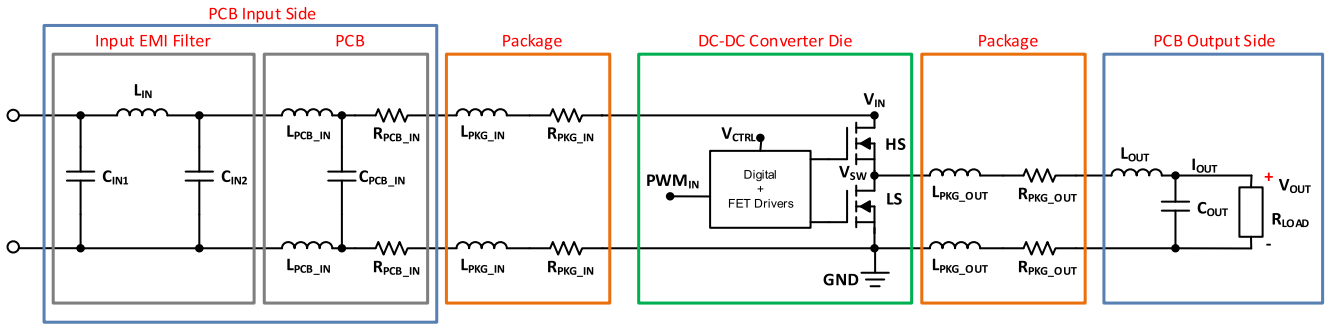

Fig. 5. Multiscale system-level transient analysis setup of the synchronous step-down DC/DC Converter.

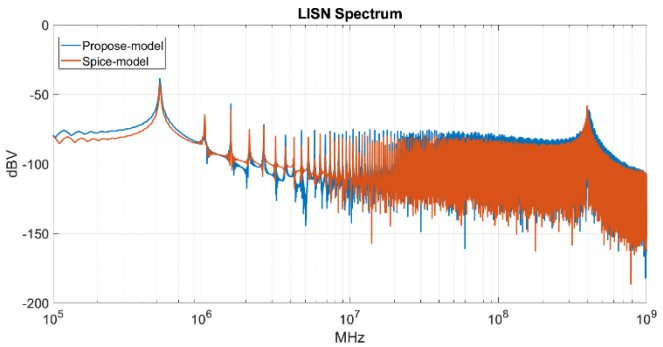

Fig. 6. Correlation of frequency domain waveforms obtained from non-linear time domain simulation of stand-alone PCB vs. full-system.

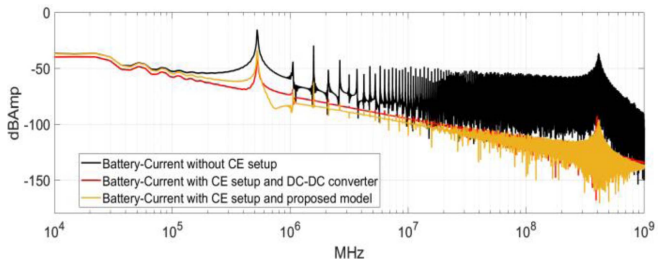

Fig. 7. The battery current was obtained in different methods (a) standalone PCB connected to the battery (b) PCB and full-system using actual IC and (c) PCB and full-system using waveform sources.

is captured by the industry-standard BSIM models. The contribution of the gate to drift region capacitance to EMI and its dependence on Vgs and Vds is captured by a proprietary model based on empirical measurements. The reverse recovery characteristics of MOSFETs are quantified by three parameters: the reverse recovery time (trr), the reverse recovery current (Irr), and the reverse recovery charge (Qrr). The impact of the reverse recovery current is modeled using a proprietary model that captures Irr accurately. The reverse recovery current interacts with the package and PCB's parasitic inductances to create voltage spikes and EMI through the relationship, V = L x (dIrr/dt). As such, the package and PCB routings are designed to optimize the voltage spike by reducing inductances in the frequency bands of interest of the device under test (~70 MHz – 200 MHz). Accurate S-parameter models of the surface-mount devices (e.g., capacitors, inductors) are employed. The package and PCB are modeled and extracted using a 3D full-wave simulator or in some cases even with a 3D quasi-static simulator. One of the primary challenges in such an approach is the convergence of the non-linear time-variant simulation with the macro-modeled S-parameters, especially with a high number of ports as may arise due to multiple cables. To alleviate this challenge a stand-alone PCB-only simulation generates the waveforms.

As demonstrated in Fig. 6, the frequency domain IC-waveforms of the stand-alone PCB simulation are roughly identical to a full-system simulation. This can be also explained by the high impedance of the cable network. Although the IC-model waveforms are invariant between a stand-alone PCB vs. full-system, the LISN voltage or the electric field results depend significantly on the cable, LISN, and additional laboratory equipment, as shown in Fig. 7.

Furthermore, the voltage source waveforms at V_{IN} and V_{SW} changes with the operating condition of the switcher. Therefore, it is critical to ensure the stimuli are captured under correct switching conditions to improve the correlation with measurement. It is also essential to capture the phase and the amplitude as the field at the antenna is the sum of the individual contribution from high-side and low-side signals.

B. Stage-2: System-Level CE/RE Simulation Using IC-Model

The electric field measured at the antenna, namely $E_{antenna}$ can be expressed as a superposition of contributions from the two equivalent voltage sources:

$$E_{antenna} = H_{Vsw} * FFT_{Vsw} + H_{Vin-Vsw} * FFT_{Vin-Vsw} \quad (1)$$

where H_{Vsw} and $H_{Vin-Vsw}$ represent the electric field generated by a 1V source over all frequencies at *Vsw* and *Vin-Vsw* respectively. FFT_{Vsw} and $FFT_{Vin-Vsw}$ represent the frequency domain spectrum of the waveforms at *Vsw* and *Vin-Vsw*. Figs. 8 and 9 below show examples of the V_{IN} and V_{IN} - V_{SW} in time and frequency domains respectively.

The system-level modeling methodology developed and implemented here is formulated through a 3D full-wave electromagnetic setup miming a virtual EMC laboratory platform. In order to reduce the time and memory bottleneck of a large-scale 3D electromagnetic simulation, parts of the EMC laboratory e.g., LISN, antenna, and EMI-receiver, are pre-characterized.

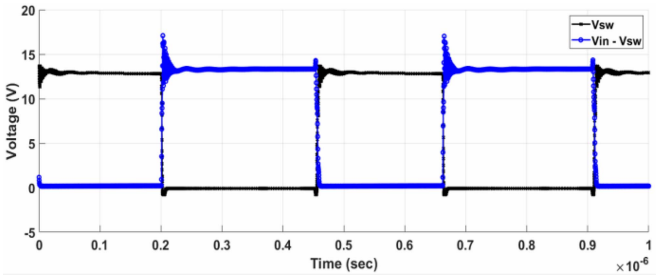

Fig. 8. Time-domain example of V_{IN} and (V_{IN} – V_{SW}) waveforms that are extracted from top-level functional simulation in system-level circuit analysis.

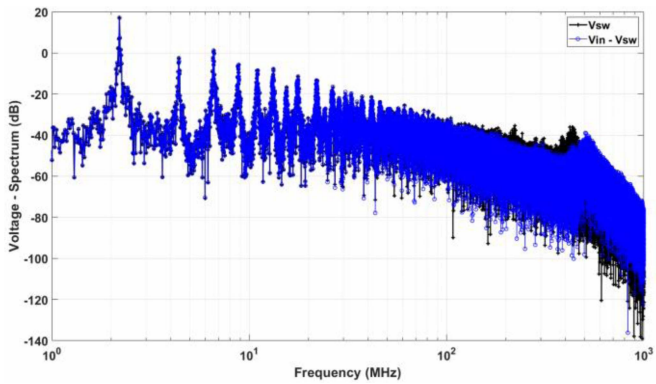

Fig. 9. FFT of an example of V_{IN} and (V_{IN} – V_{SW}) waveforms that are extracted from top-level functional simulation in system-level circuit analysis.

1) LISN Macro-Model: A LISN (line impedance stabilization network) is employed to provide a defined, stable impedance to the power input of the EUT to perform conducted emission for CISPR 25. Typically, there are primarily three main functions of LISNs. These divert unwanted signals from a power source, provide a 50Ohm coaxial port for RF noise measurement, and resist an electric circuit or component to an alternating current (impedance). The LISN may be modeled using a SPICE subcircuit as shown in Fig. 10. Additionally, the LISN model may also be generated from VNA (virtual network analyzer) characterization to extract the 2-port s-parameter frequency-dependent impedance model of the LISN.

In CISPR 25 test setup, the cable at the loadbox typically has a bend as shown in Fig. 11(b). The extracted s-parameter model is connected between the cable and the table using the lumped port. The lumped port provides high inductance due to its thinner dimension. In an actual setup, the connection is provided through a metal strip as the model in Fig. 11(c). It is important to replicate the metal dimensions of the LISN to accurately predict the RE behavior sensitive to such small inductance values. The extra bend, as shown in Fig. 11(b) has an impact on the measured emissions. The electric field with and without the extra bend at the loadbox side is shown in Fig. 12. The impact of the 3D loadbox model on the field is shown in Fig. 13.

2) EMC Chamber Model: In the CISPR 25 RE test setup, the table is placed 900mm above a conducting floor. The antenna is at a distance of 1 meter from the cable center. In PDE-based

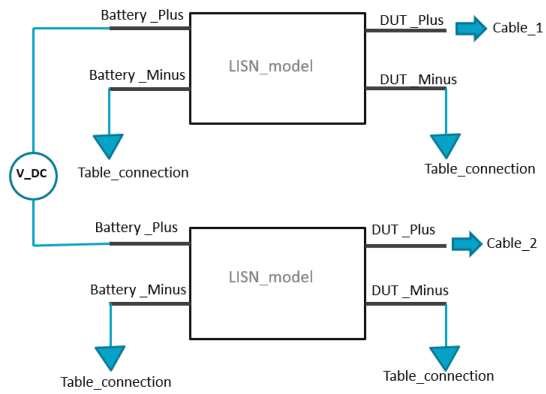

(a)

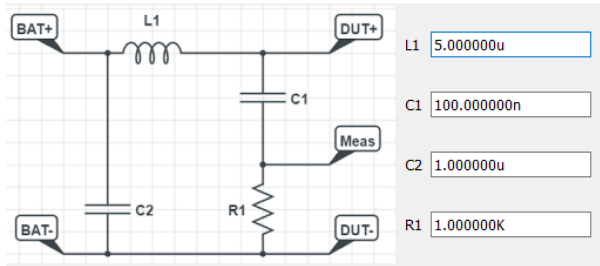

(b)

Fig. 10. Schematic model of LISN (a) 2 LISN connected to cables (b) SPICE representation of each LISN.

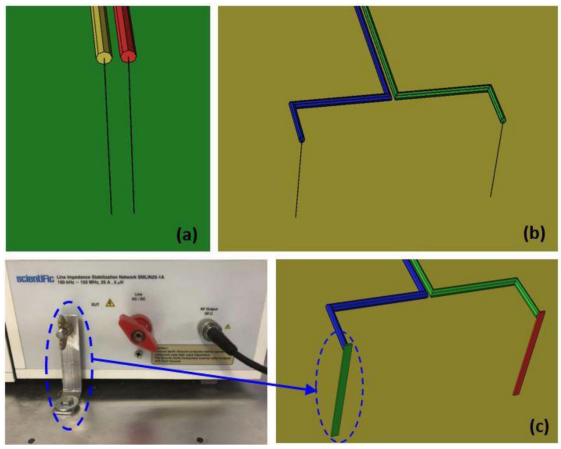

Fig. 11. Different loadbox configurations (a) default setup (b) cable bend at loadbox, and (c) solid loadbox model.

methods, an absorbing boundary is required for the solution, and the absorbing boundary's choice may affect the results unless a very-large boundary is constructed. On the other hand, the radiation condition is automatically enforced through the underlying Green's Function in a MoM-based solver. To show the effect of the size of the absorbing boundary box on the electric field results in FEM, a simple microstrip is considered in the CISPR 25 test setup. Fig. 14 shows the test setup.

The vertical electric field at the antenna location with different absorbing box sizes is shown in Fig. 15. As seen from the

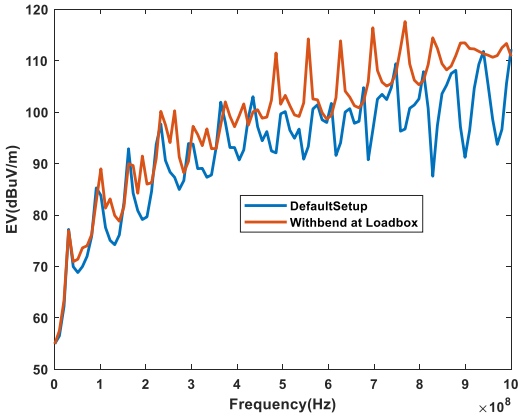

Fig. 12. Electric field comparison with and without bend at loadbox.

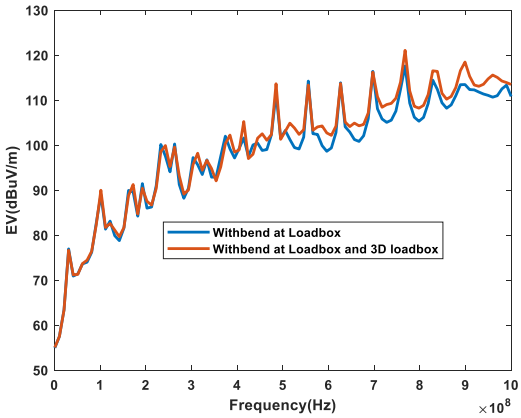

Fig. 13. Electric field comparison with and without 3D Loadbox.

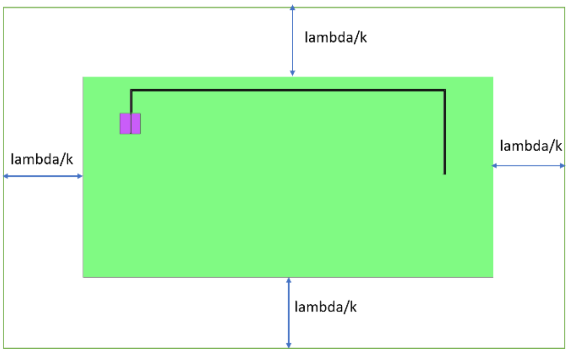

Fig. 14. CISPR25 RE test setup with absorbing boundary box, lambda is the wavelength at the highest simulation frequency (1GHz) and k = 24,8.

figure, results converge with increasing the box size, and the field with a bigger box matches well with the MoM approach. The MoM, therefore, captures an open area test site (OATS) configuration.

3) Model Summary: Table I summarizes all the appropriate components (viz. FETs, package, EVM, surface-mount technologies, test setups, among others) for CISPR 25 conducted and radiated emissions.

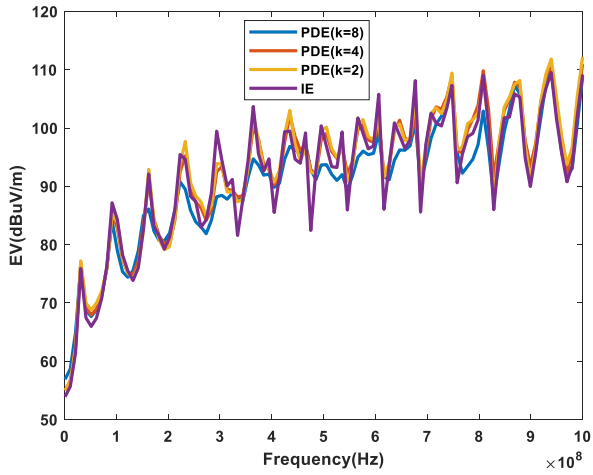

Fig. 15. Electric field with different box sizes for PDE and IE techniques.

TABLE I
LIST OF COMPONENTS MODELS

Component	CE Model	RE Model
Harness	2D TLM method	3D Full-wave
LISN	Spice	Touchstone
DUT	3D Full-wave	3D Full-wave
Passives	Spice/Touchstone	Spice/Touchstone
IC	Voltage/Current waveforms	Voltage/Current waveforms

4) 3D Full-Wave Electromagnetic Solver: An Integral Equation (IE)-based formulation, like the method of moments (MoM) has the advantage of using a surface-based mesh pertaining to the 3D geometry under consideration. This is unlike the Partial Differential Equation (PDE)-based methods such as Finite Element Method (FEM) or Finite Difference Time Domain (FDTD) method, where the medium will also need to be discretized using volume elements. This results in a relatively smaller number of mesh elements required for convergence in results. However, MoM faces the challenge of a dense matrix which is overcome by using a low-rank compression-based fast solver. This work uses commercially available EMC-focused low-rank MoM solver solutions as detailed in [33] based on the surface [34] and volume [35] based Electric Field Integral Equation. Furthermore, the walls of the anechoic chamber are not modeled in this formulation and hence any reflection from the chamber walls is neglected.

IV. CISPR 25 EMISSIONS MEASUREMENT SETUP

Emission measurements were done according to CISPR 25 test setup [6]. Both conducted and radiated emissions were performed in UL Certified EMC test laboratories. The following two sections provide details for each emission measurement. Additional comparative EMI test standards and specifications for automotive are described in [36].

A. Conducted Emissions–Voltage Method (CISPR 25)

The conducted emission measurements setup follows the CISPR 25 conducted emission (CE) specification [6]. Measurements were performed in an EMC-shielded chamber. The

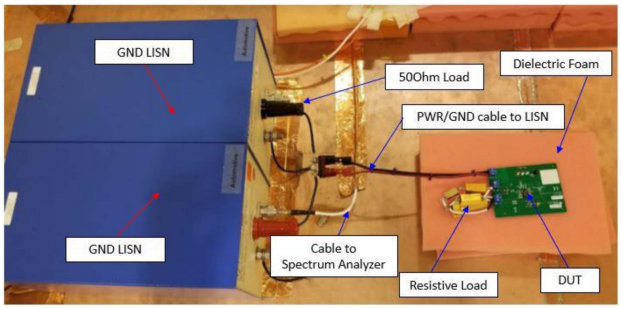

Fig. 16. CISPR 25 conducted emission measurement setup.

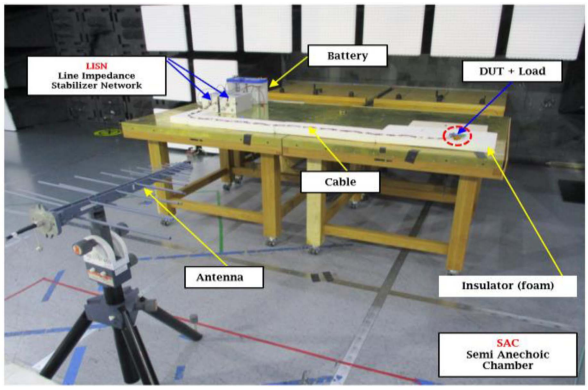

Fig. 17. CISPR 25 radiated emission measurement setup.

device-under-test (DUT) was mounted on a non-conductive, low-permittivity material at a distance of 50 mm above the reference ground plane. The power (PWR) and ground (GND) cable assembly, 200 mm long, connects the DUT PWR/GND connector to the PWR/GND LISNs. A 12V DC battery is connected to the backside of the LISN as the main power supply and a 1.2Ohm, 50W resistor is connected to the output of the device as the resistive load. The emission measurements can be performed either on the Power (PWR) or the (GND) line. When the measurements are taken on the PWR line, as shown in Fig. 16, the PWR LISN measurement port is connected to the spectrum analyzer, and the GND LISN measurement port is terminated with 50Ohm Load. The conducted emission measurements frequencies range from 15 kHz to 108 MHz.

B. Radiated Emissions

For the radiated emission (RE) measurements, the DUT, test harness, and equipment all follow the CISPR 25 test specifications [6]. All measurements were done in a 3 m semi-anechoic EMC-certified test laboratory with absorber material lining the walls and ceiling as per the standard, as shown in Fig. 17. Different antennas were used to measure emissions at the different frequency ranges of interest. These are a Rod antenna (0.15 MHz to 30 MHz), a Biconical antenna (30 MHz to 200 MHz), and a log-periodic (200 MHz to 1 GHz). Both horizontal and vertical antenna polarization measurements were performed per the standard. For this work, we focus on the (300 MHz-1 GHz) radiated emission as most of the radiated energy of the DUT is in that range.

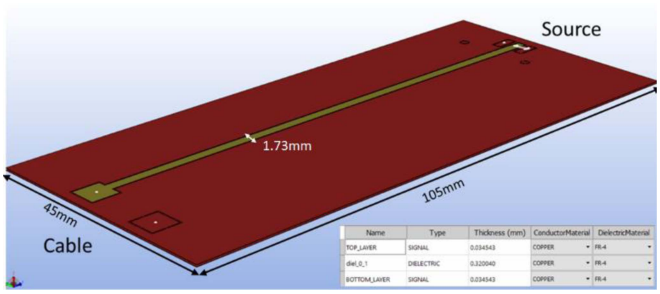

Fig. 18. A canonical microstrip PCB is used as DUT.

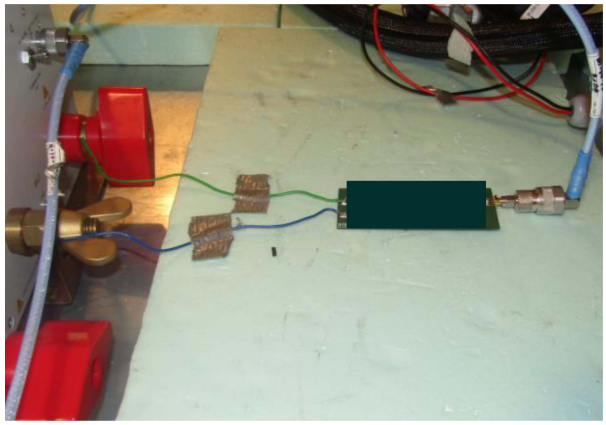

Fig. 19. A canonical microstrip PCB in CISPR25 CE setup.

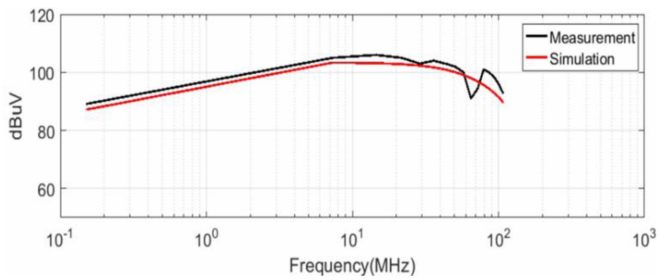

Fig. 20. Measurement and simulation correlation for the microstrip DUT in CISPR25 setup.

V. Simulation to Measurement Validation

In this section, the comparisons between laboratory measurements and simulated conducted and radiated are presented.

A. Canonical Example With Microstrip

A simple microstrip PCB, as shown in Fig. 18, is considered as a DUT for this example. One end of the microstrip is fed by a signal generator of strength 0 dBm. The CISPR 25 CE setup is shown in Fig 19.

The measured results are correlated using the proposed simulation environment, as shown in Fig. 20.

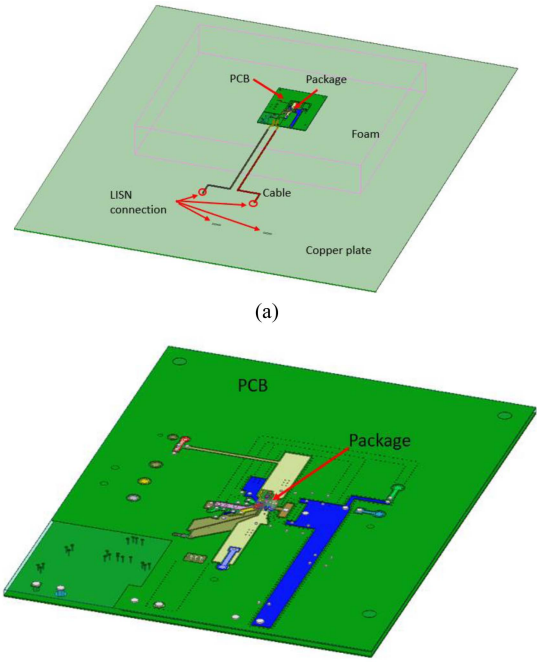

Fig. 21. Models considered for non-linear time-varying simulation: (a) Full laboratory setup and (b) standalone DUT.

B. Automotive Synchronous Step-Down Converter

1) IC-model Generation: The IC switching waveforms are generated using a non-linear time-varying (NLTV) simulation. In Fig. 21, two structures used for the NLTV simulation is described. In Fig. 21(a), the DUT, along with the parasitic model of the cable and the schematic model of the LISN is used. In Fig. 21(b), the standalone DUT is used for the simulation. As can be seen from Fig. 22(a), the simulation corresponding to Fig. 21(a) demonstrates stability and convergence issues while that for Fig. 22(b) runs successfully, as shown in Fig. 21(b). These stability issues can be handled using advanced numerical methods in reduced order modeling. However, the observation from Fig. 6 alleviates the necessity of a full-system simulation in stage-1 thereby, eliminating the risk of convergence of the NLTV simulation.

2) Conducted Emissions (CE) Correlation: Fig. 23 shows the conducted emission (CE) voltage method comparative analysis. It is evident that a good correlation has been achieved between measurement and simulation across the frequency range.

3) Radiated Emissions Correlation: Correlating radiated emission simulation to UL EMC-certified testing laboratory measurements can be more challenging than conducted emission. Our RE measurement setup is per the CISPR 25 requirement, except that the load is off-board. As shown in Fig. 24(a) and (b), to accommodate the 1.2Ohm bulky resistive load, a wire loop was soldered to the appropriate output pins of the on-board converter and assembled on a ceramic tile to dissipate heat. The loop area formed by the additional wire connection to the resistive load is not typical of CISPR 25 RE setup. Therefore, it was determined that investigating its impact, particularly

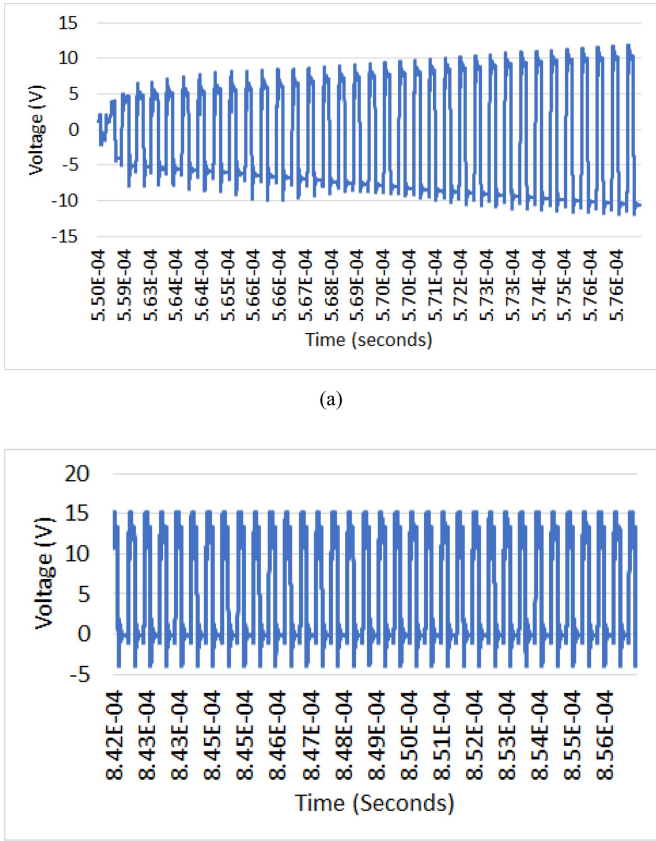

Fig. 22. NLTV simulation results for (a) full laboratory setup and (b) standalone DUT.

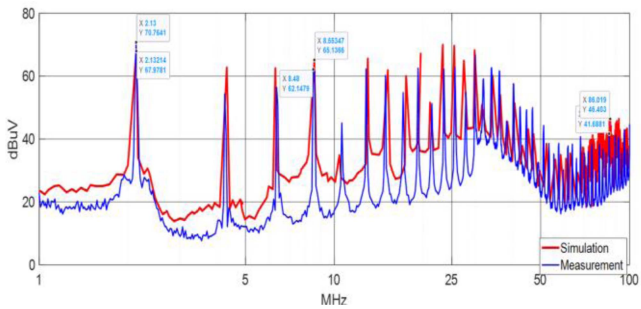

Fig. 23. CISPR 25 Conducted emission measurement vs simulation. Measurements are shown in blue and the simulation in red.

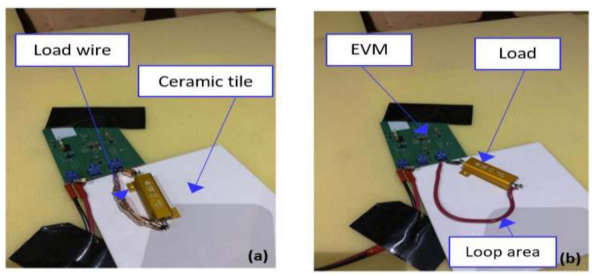

Fig. 24. Load connectivity RE measurement configuration with (a) shorter and (b) longer wire loop area.

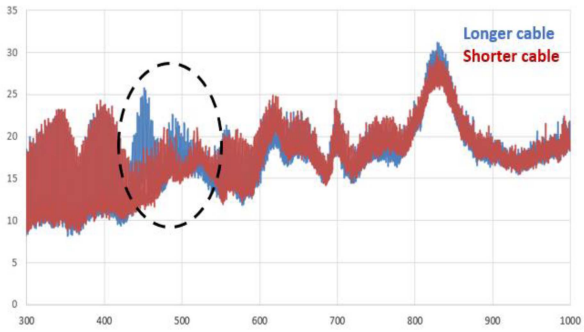

Fig. 25. CISPR 25 radiated emission measurement comparison between smaller and larger resistive load wire loop area.

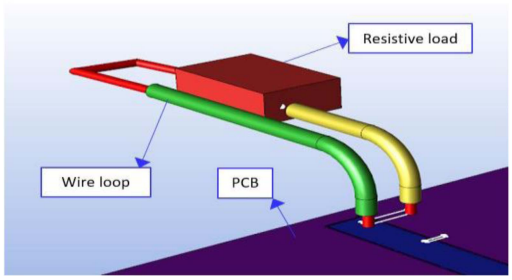

Fig. 26. Physical model of the loop wire connectivity of the off-board load.

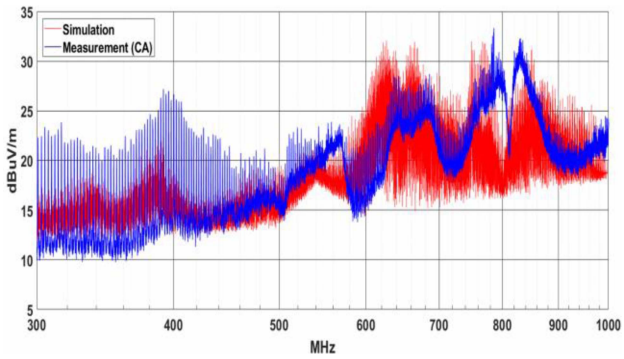

Fig. 27. CISPR 25 Radiated emission measurement vs simulation. Measurements are shown in blue and the simulation in red.

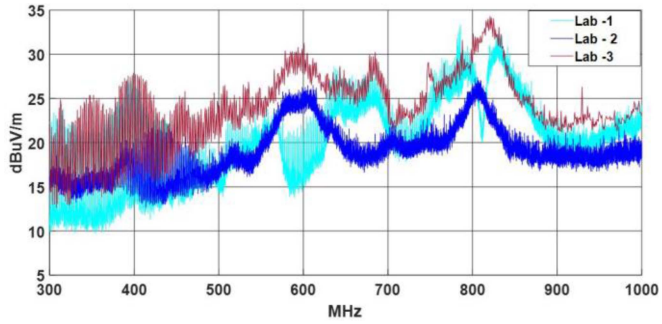

Fig. 28. Inter-labs measured CISPR 25 radiated emission at three different EMC-certified test sites.

the coupling to the supply harness, on the system emission is warranted.

To that end, emission measurements were conducted to assess the impact of the increase in the wire loop area. Based on the measured radiated emission of Fig. 25, the larger wire loop area, as suspected, modifies the radiated emission of the system, particularly in the frequency ranges of (450–525 MHz) and (820–850 MHz) respectively.

With these findings, the need to capture the exact physical configuration of the wire loop connectivity of the resistive load, as an additional component, in the system simulation was deemed critical. Fig. 26 below shows the physical model that was developed for the load connection. This was implemented in the system-level modeling and analysis as detailed in Section IV-A.

The system-level simulation is performed with a complete 3D model for the load wire and connectivity. As shown in Fig. 27, a good correlation is observed between simulation (red) and measurement (blue) for radiated emission. The simulated resonant frequency peaks locations are aligned well with peaks in measurement. A +/- 6 dB in peak amplitude is observed between simulation and measurement. Considering that the measured radiated emission data variations published in the literature are within a margin of 10 dB, the findings here are well aligned.

Previous researchers have pointed out significant differences exist across different chambers, although both are CISPR 25 compliant. A similar investigation was performed for this synchronous step-down converter device. Fig. 28 below shows the CISPR25 RE comparative measurements at three EMC-certified laboratories. Subtle differences can be observed from the comparative lab-to-lab radiated emission measurements. Lab-1 does not show the 600–650 MHz resonant peak seen in Lab-2 and Lab-3 measurements. All three sites recovered the 350–425 MHz LC resonant peak. The LC resonant peak is formed from the VIN and GND supply inductive (L) loop with the output capacitances of the power switch FETs. A maximum difference of (7-8) dB is observed at the 800–850 MHz peaks between Lab-2 and Lab-3. The findings of the inter-laboratory emission differences observed here agree with previous findings [37], [38], [39], and [40].

VI. Conclusion

A robust two-stage multiscale system-level modeling and analysis methodology for predicting CISPR 25 conducted emission (CE) and radiated emission (RE) have been developed in this work. In Stage 1, the IC model is extracted by either measurement or time-domain simulation of the stand-alone PCB, thereby avoiding the complexity of the full CISPR25 system setup. In Stage 2, the IC model and every component in the system are modeled or characterized and employed in the virtual EMC platform. Silicon validation of the predictive modeling methodology is demonstrated using a “low-EMI,” high-performance DCDC automotive synchronous step-down converter. Good correlations between modeling and EMC-certified testing laboratory emission measurements are achieved (i.e., within +/- 3 dB for CE and +/- 6dB for RE). As shown in Table II, the work detailed here contributes to advancing the current state-of-the-art in multiscale EMC modeling. The benefits of the two-stage approach are numerous, notably, the ability to perform full non-linear time variant (NLTV) analysis in Stage 1 with highly accurate device-level Physics models of the

TABLE II
COMPARISON OF THIS WORK WITH RESPECT TO EXISTING LITERATURE

Reference	[14] (Radchenko et al., 2014)	[21] (Oganezova et al., 2015	[17] (Jia et al., 2016)	[20] (Hillenbrand et al., 2017)	[24] (Song et al., 2019)	This work
Method	Uncoupled (Transfer Function Method)	Single-Stage Coupled (Behavioral switch model + lumped circuit models)	Uncoupled (Current Scan Method)	Two-Stage Coupled (Analytical switch model + 3D linear)	Single-Stage Coupled (Behavioral switch model + 3D linear)	Two-Stage Coupled (Device Physics switch model + 3D linear)
Automotive EMC Test	CISPR 25	CISPR 25	CISPR 25	CISPR 25	CISPR 25	CISPR 25
Emission type CE – Conducted Emission RE – Radiated Emission	RE	CE & RE	RE	CE & RE	CE	CE & RE
Sim. vs Meas. Correlation	5dB delta (30MHz-1GHz) for RE	+/3-9dB delta for CE and RE*	4-5dB delta (30MHz-1GHz) for RE	+/- 3dB (< 40MHz) for CE + RE	~7dBuV (50-80MHz) for CE	+/- 3dBuV for CE and +/- 6dBuV for RE
Notes	Does not comprehend interactions of coupled NLTV switch circuit on emission	Does not include 3D model of system (package + PCB)	Does not include NLTV circuit. Use a 1V, 50Ohm source impedance	Correlation only up to 110MHz	Only applicable to CE and impact of NLTV unknown for RE	Step 1 can be performed with full NLTV circuit + package and PCB system

* Results inferred from published data (not stated in paper explicitly)

MOSFETs and full 3D field analysis of the system. In addition, the predictive EMC modeling methodology developed here can be implemented, early in the design phase to ensure first-pass device EMC compliance. Various possible continuations of this work can be undertaken to improve simulation to measurement correlation, particularly for radiated emission. These include accounting for reflection and scattering off the anechoic chamber walls, accurate characterization of the dielectric foam insulation, and access to accurate s-parameter models of EMC-certified test site equipment.

REFERENCES

[1] M. Ramdani et al., "The electromagnetic compatibility of integrated circuits—Past, present, and future," *IEEE Trans. Electromagn. Compat.*, vol. 51, no. 1, pp. 78–100, Feb. 2009, doi: 10.1109/TEMC.2008.2008907.

[2] S. Schulz, P. Kanschat, and A. Lindemann, "EMI prediction of power converters using switching waveform analysis," in *Proc. IEEE 7th Int. Conf. Integr. Power Electron. Syst.*, 2012, pp. 1–5.

[3] K. M. Muttaqi and M. E. Haque., "Electromagnetic interference generated from fast switching power electronic devices," *Int. J. Innov. Energy Syst. Power*, vol. 3, no. 1, pp. 19–26, Apr. 2008.

[4] A. Domurat-Linde and E. Hoene, "Analysis and reduction of radiated EMI of power modules," in *Proc. IEEE 7th Int. Conf. Integr. Power Electron. Syst.*, 2012, pp. 1–6.

[5] M. Shousha, D. Dinulovic, M. Brooks, M. Hofer, and M. Haug, "Design and application considerations of packaging of DC-DC converter micromodules," in *Proc. IEEE Appl. Power Electron. Conf. Expo.*, 2021, pp. 2318–2322, doi: 10.1109/APEC42165.2021.9487309.

[6] *Vehicles, Boats and Internal Combustion Engines – Radio Disturbance Characteristics – Limits and Methods of Measurement for the Protection of On-Board Receivers*." CISPR 25:2016, CISPR: Geneva, Switzerland, Oct. 2017.

[7] M. Zhou, J. Li, Q. Wang, Y. Zhang, X. Wang, and S. He, "Challenges of multi-scale modelling for system-level EMI simulation," in *Proc. IEEE Int. Symp. Electromagn. Compat. Asia-Pacific Symp. Electromagn. Compat.*, 2018, pp. 145–150, doi: 10.1109/ISEMC.2018.8394097.

[8] F. Zare., "EMI issues in modern power electronic systems," *IEEE Electromagn. Compat. Soc. Newsletters*, vol. 221, pp. 53–58, 2009.

[9] A. Barchanski, J. Kraemer, and P. Luzzi, "EMC simulation in the design flow of modern electronics," *Microw. J.*, vol. 57, no. 12, pp. 88–94, 2014.

[10] A. Durier, C. Marot, and O. Crepel, "Using the EM simulation tools to predict the conducted emissions level of a DC/DC boost converter: Introducing EBEM-CE model," in *Proc. IEEE 9th Int. Workshop Electromagn. Compat. Integr. Circuits*, 2013, pp. 152–157, doi: 10.1109/EMCCompo.2013.6735191.

[11] C. Bleoju, A.-M. Silaghi, and A. D. Sabata, "Simulation and measurement of conducted emissions–Current probe in automotive EMC," in *Proc. IEEE Int. Symp. Signals, Circuits Syst.*, 2021, pp. 1–4, doi: 10.1109/ISSCS52333.2021.9497406.

[12] A. Apelsmeier, C. Rettner, and M. März, "Model for conducted emission of SiC power modules for automotive traction inverter-comparison to behaviour-based model," in *Proc. IEEE 21st Workshop Control Model. Power Electron.*, 2020, pp. 1–8, doi: 10.1109/COMPEL49091.2020.9265805.

[13] F. A. Kharanaq, A. Emadi, and B. Bilgin, "Modeling of conducted emissions for EMI analysis of power converters: State-of-the-art review," *IEEE Access*, vol. 8, pp. 189313–189325, 2020, doi: 10.1109/ACCESS.2020.3031693.

[14] A. Radchenko et al., "Transfer function method for predicting the emissions in a CISPR-25 test-setup," *IEEE Trans. Electromagn. Compat.*, vol. 56, no. 4, pp. 894–902, Aug. 2014, doi: 10.1109/TEMC.2013.2297303.

[15] S. Hrigua, F. Costa, C. Gautier, and B. Revol, "New modeling method based on transfer functions for EMI analysis in power electronic converters," in *Proc. IEEE Int. Symp. Electromagn. Compat.*, 2012, pp. 1–6, doi: 10.1109/EMCEurope.2012.6396839.

[16] D. Schneider, S. Tenbohlen, and W. Köhler, "Pre-compliance test method for radiated emissions of automotive components using scattering parameter transfer functions," in *Proc. IEEE Int. Symp. Electromagn. Compat.*, 2012, pp. 1–6, doi: 10.1109/EMCEurope.2012.6396690.

[17] J. Jia, D. Rinas, and S. Frei, "Predicting the radiated emissions of automotive systems according to CISPR 25 using current scan methods," *IEEE Trans. Electromagn. Compat.*, vol. 58, no. 2, pp. 409–418, Apr. 2016, doi: 10.1109/TEMC.2015.2511185.

[18] S. Dhar, K. Patra, S. Nair, L. Kumar, S. Krishnan, and B. P. Nayak, "Prediction of radiated emission with transmission line model for CISPR 25," in *Proc. IEEE Asia-Pacific Int. Symp. Electromagn. Compat.*, 2021, pp. 1–4, doi: 10.1109/APEMC49932.2021.9596647.

[19] J. Jia, Z. Lai, R. Wang, and X. Li, "Predicting radiation of CISPR 25 complaint ALSE environment," *Appl. Comput. Electromagn. Soc. J.*, vol. 34, no. 8, pp. 1226–1233, Aug. 2019.

[20] P. Hillenbrand, M. Beltle, S. Tenbohlen, and J. Hansen, "Transient co-simulation of electromagnetic emissions caused by a SiC traction inverter," in *Proc. IEEE Int. Symp. Electromagn. Compat.*, 2017, pp. 1–6, doi: 10.1109/EMCEurope.2017.8094649.

[21] I. Oganezova, R. Kado, B. Khvitia, A. Gheonjian, and R. Jobava, "Simulation of conductive and radiated emissions from a wiper motor according to CISPR 25 standard," in *Proc. IEEE Int. Symp. Electromagn. Compat.*, 2015, pp. 963–968, doi: 10.1109/ISEMC.2015.7256296.

[22] B. Wunsch, S. Skibin, V. Forsstrom, and I. Stevanovic, "EMC component modeling and system-level simulations of power converters: AC motor drives," *Energies*, vol. 14, 2021, Art. no. 1568, doi: 10.3390/en14061568.

[23] G. Frantz, D. Frey, J. L. Schanen, B. Revol, H. Bishnoi, and P. Mattavelli, "EMC models for power electronics: From converter design to system level," in *Proc. IEEE Energy Convers. Congr. Expo.*, 2013, pp. 4247–4252, doi: 10.1109/ECCE.2013.6647267.

[24] C. Song, H. Kweon, U. Lee, J. Kim, S. Yang, and J. Park, "Modeling of conducted EMI noise in an automotive LED driver module with DC/DC converters," in *Proc. IEEE Int. Symp. Electromagn. Compat.*, 2019, pp. 1009–1013, doi: 10.1109/EMCEurope.2019.8872093.
[25] R. Murugan et al., "System-level SoC near-field (NF) emissions: Simulation to measurement correlation," in *Proc. IEEE Electron. Compon. Technol. Conf.*, 2012, pp. 140–146.
[26] A. Gupta and K. Wiggenhorn, "Enhanced HotRod^{TM} QFN package: Achieving low EMI performance in industry's smallest 4-A converter," Texas Instrum., Dallas, TX, USA, Appl. Rep. SNVA935A, Jun. 2020.
[27] T. Hegarty, "Reduce buck-converter EMI and voltage stress by minimizing inductive parasitics," *Analog Appl. J.*, vol. 3, pp. 1–7, 2016.
[28] A. Bhargava, D. Pommerenke, K. W. Kam, F. Centola, and C. W. Lam, "DC-DC buck converter EMI reduction using PCB layout modification," *IEEE Trans. Electromagn. Compat.*, vol. 53, no. 3, pp. 806–813, Aug. 2011, doi: 10.1109/TEMC.2011.2145421.
[29] K. W. Kam, D. Pommerenke, C.-W. Lam, and R. Steinfeld, "EMI analysis methods for synchronous buck converter EMI root cause analysis," in *Proc. IEEE Int. Symp. Electromagn. Compat.*, 2008, pp. 1–7, doi: 10.1109/ISEMC.2008.4652125.
[30] S. Wu et al., "Investigation of noise coupling from switching power supply to signal nets," in *Proc. IEEE Int. Symp. Electromagn. Compat.*, 2010, pp. 79–84, doi: 10.1109/ISEMC.2010.5711251.
[31] N. Zhang, D. Li, V. Zhang, and A. Chen, "Reduce conducted EMI in automotive buck converter," Texas Instruments, Inc., Dallas, TX, USA, Appl. Rep. SNVA886, Jul. 2019.
[32] R. Bramanpalli, "The behavior of electromagnetic radiation of power inductors in power management," *Wurth Electronik Appl. Note*, vol. 47, 2017.
[33] D. Gope and V. Jandhyala, "Efficient Solution of EFIE via Low-Rank Compression of Multilevel Predetermined Interactions," *IEEE Trans. Antennas Propag.*, vol. 53, no. 10, pp. 3324–3333, Oct. 2005.
[34] S. Rao, D. Wilton, and A. W. Glisson, "Electromagnetic scattering by surfaces of arbitrary shape," *IEEE Trans. Antennas Propag.*, vol. 30, no. 3, pp. 409–418, May 1982.
[35] D. Schaubert, D. Wilton, and A. Glisson, "A tetrahedral modeling method for electromagnetic scattering by arbitrarily shaped inhomogeneous dielectric bodies," *IEEE Trans. Antennas Propag.*, vol. 32, no. 1, pp. 77–85, Jan. 1984.
[36] G. D'Abreu, C. Fanning, and A. Sarwar, "Automotive EMC Testing: CISPR 25, ISO 11452-2, and Equivalent Standards," in *Compliance Electronic Design, Testing & Standards*, Jan. 2016.
[37] F. Lafon, J. Davalan, and R. Dupendant, "Inter-laboratory comparison between CISPR25 chambers, identification of influent parameters and analysis by 3D simulation," in *Proc. IEEE Asia-Pacific Symp. Electromagn. Compat.*, 2015, pp. 71–74, doi: 10.1109/APEMC.2015.7175291.
[38] F. Lafon, R. Dupendant, and J. Davalan, "Investigation on dispersions between CISPR25 chambers for radiated emissions below 100 MHz," in *Proc. IEEE Int. Symp. Electromagn. Compat.*, 2014, pp. 29–34.
[39] D. Kumar and P. Sudhakar, "Inter laboratory comparison (ILC) of conducted emission measurements," *IEEE Electromagn. Compat. Mag.*, vol. 7, no. 3, pp. 52–59, Third Quarter 2018, doi: 10.1109/MEMC.2018.8479339.
[40] S. Baisakhiya, A. Albin, and B. Subbarao, "Interlaboratory comparison of radiated emission measurements," in *Proc. IEEE 10th Int. Conf. Electromagn. Interference Compat.*, 2008, pp. 283–285.

Rajen Murugan (Senior Member, IEEE) was born in Stanley, Rose-Hill, Mauritius. He received the B.Sc. (Hons.) degree in physics from The University of Winnipeg, Winnipeg, MB, Canada, in 1994, the M.Sc. degree in physics from the University of Leeds, Leeds, U.K., in 1995, and the Ph.D. degree in applied electromagnetics from the University of Manitoba, Winnipeg, in 1999. He is currently a Distinguished Member of Technical Staff with Texas Instruments, Inc., Dallas, TX, USA. He holds 28 patents (54 pending) and has authored or coauthored more than 60 papers in IEEE peer-reviewed journals and conferences. His research interests include applied computational electromagnetics, multiphysics system co-design modeling and analysis, and high-frequency/speed mixed-signal integrated circuit and package design.

Jie Chen (Member, IEEE) was born in Hubei, China. She received the B.Sc. degree in electrical engineering from the South China University of Technology, Guangzhou, China, in 2000, and the M.Sc. degree in electrical engineering from the University of Florida, Gainesville, FL, USA, in 2005. From 2006 to 2010, she was an SI/PI Engineer with Intel, Santa Clara, CA, USA. She is currently a Senior Member of Technical Staff with Texas Instruments, Inc., Dallas, TX, USA. She holds 15 patents (five pending). Her research interests include EMI/EMC predictive modeling, mitigation techniques in EMI/EMC, high voltage, current power electronics system co-design, and electrical-thermal multiphysics in complex package technologies.

Ambreesh Tripathi was born in Lucknow, India. He received the B.Tech. degree in electronics and telecommunication engineering from the National Institute of Technology, in 2008, and the MBA degree from the Hass School of Business, University of California Berkeley, Berkeley, CA, USA. He is currently a Systems Manager responsible for defining Power Products with Texas Instruments, Dallas, TX, USA, where he is also a Member of Technical Staff. He has conceptualized various EMI related innovations and is sought for the expertise across TI and has influenced definition of more than 15 ICs with added EMI related features.

Bibhu Prasad Nayak (Member, IEEE) was born in Cuttack, India. He received the B.E. degree in electronics and telecommunication engineering from the University College of Engineering, Sambalpur University, Sambalpur, India, in 2002, and the M.Tech. degree in microwave and photonics from IIT Kanpur, Kanpur, India, in 2005, and the Ph.D. degree in electrical communication engineering, Indian Institute of Science, Bengaluru, India, in 2021. He has been involved in electromagnetic compatibility simulations for automotive products at Robert Bosch Engineering and Business Solutions, Bengaluru. He is the Co-founder of SimYog Technology Pvt. Ltd., Bengaluru, a startup focused on system-level EMI/EMC simulation.

Harikiran Muniganti received the B.Tech. degree in electronics and communication engineering from the Gokaraju Rangaraju Institute of Engineering and Technology, JNTU University, Hyderabad, India, in 2009, the M.E. degree in telecommunications from Indian Institute of Science, Bengaluru, India, in 2011, and the Ph.D. degree from the Electrical Communication Engineering, Indian Institute of Science, Bengaluru, in 2022. He is the Co-founder with Simyog Technology Pvt. Ltd., Bengaluru, a startup focused on system-level EMI/EMC simulation.

Dipanjan Gope (Senior Member, IEEE) received the B.Tech. degree in electronics and electrical communication engineering from IIT Kharagpur, Kharagpur, India, in 2000, and the M.S. and Ph.D. degrees in electrical engineering from the University of Washington, Seattle, WA, USA, in 2003 and 2005, respectively. Since 2011, he has been an Associate Professor with the Department of Electrical Communication Engineering, Indian Institute of Science, Bangalore, India. He has authored more than 80 journal and conference publications. Dr. Gope is also the Co-founder of Simyog Technology Pvt. Ltd., Bengaluru, a startup focused on system-level EMI/EMC simulation.